A coupled closed-form/Doubly-Asymptotic Approximation approach for the response of orthotropic plates subjected to an underwater explosion

Ye Pyae Sone Oo, Hervé Le Sourne, Olivier Dorival

Ships and Offshore Structures

A coupled closed-form/Doubly-Asymptotic Approximation approach for the response of orthotropic plates subjected to an underwater explosion

Ye Pyae Sone Oo[a*], Hervé Le Sourne[b] and Olivier Dorival[c]

[a]*GeM Institute (UMR CNRS 6183) – Calcul-Meca, Nantes, France*
[b]*GeM Institute (UMR CNRS 6183) – Icam Nantes campus, France*
[c]*Clément Ader Institute (FRE CNRS 3687) – Icam Toulouse campus, France*

Abstract

In this paper, a closed-form analytical solution procedure is proposed to solve the coupled fluid-structure interaction (FSI) equations that involve the first-order Doubly Asymptotic Approximation (DAA_1) formulation. An efficient method comprised of the nonstandard finite difference (NSFD) scheme is applied. First of all, analytical equations are developed to analyze the response of a rigid mass-spring oscillator in an air-backed condition when it is subjected to a plane shock exponential wave coming from a far-field underwater explosion. After validating the results with LS-DYNA/USA (DAA_1), these equations are extended to determine the response of two-dimensional, simply-supported rectangular plate, and then tested on the isotropic and orthotropic plates within a small deflection regime. Parametric studies are also performed by varying the load decay times, peak pressures, as well as the aspect ratios of the plate. Finally, the advantages and limitations of the proposed formulae are exposed along with suggestions for the future work.

Keywords: Doubly-Asymptotic Approximation (DAA); Fluid-structure interaction (FSI); Underwater explosion (UNDEX); LS-DYNA/USA; Nonstandard finite difference method.

1. Introduction

Non-contact underwater explosion (UNDEX) has long been a major threat to military vessels and civil marine structures since World War II. In order to prevent immersed structures against such intense loadings, it is very important for the designers to fully understand the underlying physics such as shock wave propagation, fluid-structure interaction (FSI), bulk cavitation, and so on. Over the past few decades, advanced numerical approaches involving Underwater Shock Analysis (USA) code have been widely utilized to analyze the underwater shock structure interaction problems. The fluid equations solved by USA code employ Doubly Asymptotic Approximation, a boundary element method proposed by (Geers 1978) during 1970s. These are time domain differential equations that approach exactness at both low and high frequencies, allowing for a smooth transition in-between. The governing equations are expressed in terms of wet surface variables only and thus, it is not required to explicitly model the surrounding fluid. Traditionally, these equations have been solved numerically with the use of a staggered solution procedure and been incorporated into various commercial finite element tools such as LS-DYNA, NASTRAN (DeRuntz 1989). These numerical tools are indeed very powerful. However, as investigated by (Barras 2012), they can be very time consuming and demand much competence from the users. Consequently, they are not suitable for the preliminary design phases in which numerous loading scenarios as well as different structural configurations need to be tested. In this regard, simplified analytical solutions become more relevant since they provide reasonably accurate solutions in a relatively short amount of time as well as good insights to the problems.

* Corresponding author. Tel.: +33-0-240524827.
E-mail address: ye-pyae.sone-oo@icam.fr

Nomenclature

A_f	the (wetted) surface area of the plate
c_w	speed of sound in water (fluid)
h	thickness of the plate
m, n	mode numbers in x- and y-directions respectively
M_f	water-added mass per unit area
m_s	areal mass of the plate
P_0	peak pressure
P_i	incident pressure
P_s	scattered pressure
ψ_x, ψ_y	rotation of the transverse normal about y- and x-axes respectively
P_{tot}	the total pressure acting on the plate
ρ_s	density of the plate
ρ_w	density of water (fluid)
t	time
τ	decay time of the loading
u_i	particle velocity of the incident wave
u_s	particle velocity of the scattered wave
w	transverse displacement
x, y, z	Cartesian coordinate system

2. Background

Underwater explosions not only generate a primary shock wave that propagates through the surrounding fluid medium at the speed of sound but also cause the formation and oscillation of a gas bubble. Depending on the standoff distance and the charge mass, these can be characterized as near-field or far-field explosions. In this paper, it is assumed that the target plate is at a sufficiently far standoff distance from the explosive charge so that the pressure can be regarded as a plane shock wave and the secondary pressure wave caused by the bubble pulsation can be ignored. According to (Cole 1948), the plane shock pressure wave can be expressed as:

$$P(t) = P_0 e^{-t/\tau}, \quad for\ 0 \le t \le \tau \tag{1}$$

where P_0 is the peak pressure, t is the time variable, and τ is the decay time required for the peak pressure to fall to $1/e$ of its peak value. The corresponding peak pressure P_0 and the decay time τ can be determined from the charge mass C, standoff distance R and the type of the explosive charge by using the Principle of Similarity as follows (Cole 1948):

$$P_0 = K_1 \left(\frac{C^{1/3}}{R}\right)^{A_1}, \qquad \tau = K_2 C^{1/3} \left(\frac{C^{1/3}}{R}\right)^{A_2} \tag{2}$$

where K_1, A_1, K_2 and A_2 are constants that depend on the types of the explosives.

The arrival of the plane shock wave to the target structure would bring about an interaction phenomenon in which the total pressure at the interface can be obtained by a linear superposition of the incident and scattered pressures. The scattered pressure involves reflection of the incident pressure after the impact and damping radiation caused by the sudden movement of the plate. This is called high frequency or early-time interaction phenomenon and its solution was proposed by (Taylor 1941) in which the plate is either free-standing or supported by a linear spring. Taylor's theory, however, did not take into account the late-time phenomenon or the cavitation effect. The former effect can be associated to an additional pressure created during the plate deceleration phase while the latter should be accounted for when the total pressure in the fluid drops below the vapor pressure. Nevertheless, due to the simplicity and effectiveness of Taylor's solutions, there have been many research efforts in the past that used Taylor's FSI formulations to idealize the underwater blast as an impulsive loading, for example, (Hutchinson and Xue 2005; Brochard *et al.* 2018, 2020). The authors have also applied a similar approach

by dividing the FSI response stages into two: early-time and the long-time stages, see (Sone Oo *et al.* 2019). However, this kind of approach may lead to overestimation or underestimation of the plate response according to (Deshpande *et al.* 2006; Schiffer *et al.* 2012). Thus, in the recent paper of (Sone Oo *et al.* 2020), the applicability of the Taylor's 1D FSI theory in the study of underwater explosion response of orthotropic plates was investigated. Based on various case studies, it was shown that the two-step approach based on Taylor's theory is valid only for a certain range of FSI parameter.

In this regard, Doubly Asymptotic Approximations developed by (Geers 1978) may be applied so as to alleviate some of the limitations imposed by the previous two-step approach. These are the first- and second-order differential equations in time to determine the fluid pressure due to scattered wave on the fluid-structure interface. They take into account both early- and long-time structural motions as well as a smooth transition between the two. The second-order approximation (DAA_2) is a generalization of the first-order approximation (DAA_1) with enhanced accuracy. However, due to the increased complexity of DAA_2, only DAA_1 is adapted in this paper. The objective is to propose a closed-form like solution so that the coupled FSI equations of DAA_1 can be solved rapidly. This is done by adapting a nonstandard finite difference (NSFD) scheme developed by (Songolo and Bidégaray-Fesquet 2018). The use of NSFD scheme ensures the exactness of the solutions as will be seen in the next section. In what follows, analytical equations are derived to predict the response of an air-backed, spring-supported rigid plate. Then, they are extended for a 2D deformable, air-backed plate with simply-supported boundary condition. The obtained results are evaluated by comparing with those simulated in LS-DYNA/USA (DAA_1) with or without cavitation and also with the previous results available in (Sone Oo *et al.* 2020). Finally, the advantages and limitations of the proposed formulations are exposed, leaving grounds for future research.

3. Analytical models

3.1. Response of a spring-supported rigid plate

Suppose that a rigid plate having an areal mass m_s is subjected to a uniformly distributed incident shock wave $P_i(t)$. The plate is exposed to water with density ρ_w on one side and a linear spring and air on the other side, see Fig. 1. The equation of motion of a single degree-of-free (DOF) system can thus be swritten as:

$$\ddot{W}(t) + \omega^2 W(t) = \frac{P_{tot}(t)}{m_s} \tag{3}$$

where $m_s = \rho_s h$ is the areal mass of the plate; $\omega = \sqrt{K/m_s}$ is the angular frequency of the plate, K is the areal stiffness of the spring, $P_{tot}(t)$ is the total pressure subjected to the plate, and $W(t)$ is the displacement of the plate taking positive in the z-direction as shown in Fig. 1.

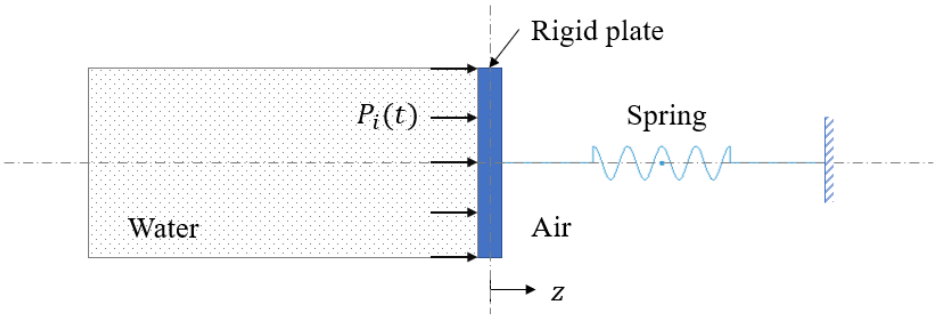

Fig. 1. A mass-spring system containing a rigid plate subjected to an incident pressure

The total pressure $P_{tot}(t)$ from Eq. (3) is determined by a linear superposition of the incident pressure $P_i(t)$ and the scattered pressure $P_s(t)$. Mathematically,

$$P_{tot}(t) = P_i(t) + P_s(t) \tag{4}$$

In this paper, the incident pressure is considered as an exponential decay form, Eq. (1). According to DAA$_1$ formulation of (Geers 1978), the scattered pressure $P_s(t)$ can be given as:

$$\dot{P}_s(t) + D_f P_s(t) = \rho_w c_w \dot{u}_s(t) \tag{5}$$

where $D_f = (\rho_w c_w)/(M_f)$ is a ratio of the acoustic impedance of water to the water-added mass per unit area of the submerged plate, and $\dot{u}_s(t) = \dot{u}_i(t) - \dot{W}(t)$ in which $\dot{u}_s(t)$ and $\dot{u}_i(t)$ are the incident and scattered accelerations of the fluid particles respectively. The expression for $\dot{u}_s(t)$ comes from the velocity continuity condition at the fluid-structure interface. M_f is the *areal* water-added mass for the rigid plate when it moves in water and can be calculated from (Blevin 1979). The system of equations becomes coupled when Eq. (5) is solved together with the structural equation, Eq. (3). The scattered pressure, particle acceleration, as well as the kinematics of the plate must be updated for each time step.

For a far-field plane shock wave, the incident pressure is related to the incident particle velocity as:

$$P_i = \rho_w c_w u_i \tag{6}$$

To discretize Eq. (3) in time domain, let us rearrange it into a system of two first-order differential equations as:

$$\begin{aligned} \dot{W} &= V \\ \dot{V} &= -\omega^2 W + \frac{P_{tot}}{m_s} \end{aligned} \tag{7}$$

Equation (7) can be expressed in matrix form as:

$$[\dot{X}] = [A][X] + [B] \tag{8}$$

where $[\dot{X}] = \begin{bmatrix} \dot{W} \\ \dot{V} \end{bmatrix}$, $[X] = \begin{bmatrix} W \\ V \end{bmatrix}$, $[A] = \begin{bmatrix} 0 & 1 \\ -\omega^2 & 0 \end{bmatrix}$ and $[B] = \begin{bmatrix} 0 \\ \frac{P_{tot}}{m_s} \end{bmatrix}$.

For the numerical approximation of Eq. (8), the interval $[t_0, t]$ is discretized into:

$$t^i = t_0 + (i-1)\Delta t \tag{9}$$

where the parameter $\Delta t > 0$ is the step size, t_0 is the initial time, t^i is the current time step, and $i = 1,2,3,\ldots$ refers to the discrete points in time. An approximate solution for $[X(t^i)]$ at time t^i is denoted here as $[X]^i$ for simplicity and can be obtained by applying an efficient numerical scheme called nonstandard finite difference (NSFD) methodology (Mickens 1993).

Definition 1. *The numerical solution for Eq. (8) is called a nonstandard finite difference method if at least one of the following conditions is satisfied:*

- *The renormalization of the step size:* $[\dot{X}]^i = \big(\phi(\Delta t)\big)^{-1}(X^{i+1} - X^i)$, *where* $\phi(\Delta t) = \Delta t I + \mathcal{O}(\Delta t^2)$ *is a positive diagonal matrix; and*
- *The nonlocal approximation of the right-hand side of Eq. (8): for example,* $[X] \to [X]^{i+1}$.

(Mickens 1993)

If $[B]$ from Eq. (8) is taken as zero, the exact numerical solution is:

$$[X]^{i+1} = \{e^{[A]\Delta t}\}[X]^i \tag{10}$$

With some algebraic manipulations, it is able to show that:

$$[\phi(\Delta t)]^{-1}([X]^{i+1} - [X]^i) = [A][X]^i \tag{11}$$

where $[\phi(\Delta t)] = \left(\left[e^{[A]\Delta t}\right] - I\right)[A]^{-1}$ which verifies the first condition of **Definition 1** on NSFD scheme. By adding the non-autonomous term to Eq. (11), the scheme becomes:

$$[\phi(\Delta t)]^{-1}([X]^{i+1} - [X]^i) = [A][X]^i + [B]^i \tag{12}$$

whose explicit form including the matrix $\left\{e^{[A]\Delta t}\right\}$ is as follows:

$$[X]^{i+1} = \left\{e^{[A]\Delta t}\right\}[X]^i + [\phi(\Delta t)][B]^i \tag{13}$$

The solution to Eq. (13) lies in finding the exponential matrix $\left\{e^{[A]\Delta t}\right\}$ which can be done by using the following linear combination (Songolo and Bidégaray-Fesquet 2018):

$$\left\{e^{[A]\Delta t}\right\} = \left(\frac{\lambda_1 e^{\lambda_2 \Delta t} - \lambda_2 e^{\lambda_1 \Delta t}}{\lambda_1 - \lambda_2}\right)[I] + \left(\frac{e^{\lambda_1 \Delta t} - e^{\lambda_2 \Delta t}}{\lambda_1 - \lambda_2}\right)[A] \tag{14}$$

where $\lambda_1, \lambda_2 = \pm\omega$ are two distinct eigen values of the $[2 \times 2]$matrix $[A]$. Solving Eq. (14) and substituting it into Eq. (13) leads to the closed-form like expressions below:

$$\begin{aligned} W^{i+1} &= W^i \cos(\omega\Delta t) + V^i \left(\frac{\sin(\omega\Delta t)}{\omega}\right) - P_{tot}^i \left(\frac{\cos(\omega\Delta t) - 1}{m_s \omega^2}\right) \\ V^{i+1} &= -W^i \omega \sin(\omega\Delta t) + V^i \cos(\omega\Delta t) + P_{tot}^i \left(\frac{\sin(\omega\Delta t)}{m_s \omega}\right) \end{aligned} \tag{15}$$

where the step size required to solve these explicit equations is estimated as $\Delta t \leq \pi/(200\omega)$, which is at most one-hundredth of the time to reach the first peak displacement. It is worth mentioning here that these closed-form like expressions ensure the exactness of the solution and can be readily solved for any initial conditions at time step t^i. Unlike the well-known Runge-Kutta scheme, the present scheme does not require additional function evaluations, thus saving more computation time, as will be shown later.

Applying the same procedure on Eq. (5), the expression for P_s for the next time step is obtained as:

$$P_s^{i+1} = P_s^i e^{-D_f \Delta t} + \left(\frac{1 - e^{-D_f \Delta t}}{D_f}\right)\left(-\rho_w c_w \dot{V}^i + \dot{P}_i^i\right) \tag{16}$$

Since the incident pressure P_i is known for all time steps, total pressure P_{tot} can be updated for each time step if Eq. (16) is solved simultaneously using Eqs. (4) and (15). The initial conditions at time step zero are taken as $W(0) = V(0) = 0$, $\dot{V}(0) = 2P_0/m_s$ and $P_s(0) = P_i(0) = P_0$. Note that cavitation can be considered by introducing a flag that would trigger whenever $P_{tot}^i \leq 0$. Following the suggestion of USA user's manual, only the scattered pressure P_s is modified whenever the cavitation criterion is met.

3.2. Response of a 2D deformable simply-supported plate

The mass-spring equation from the previous subsection is extended to determine the response of an air-backed rectangular plate in a simply-supported boundary condition when subjected to a plane shock wave in a negative z-direction, see Fig. 2. The plate is assumed to have the size (a, b) and a uniform thickness h. Cartesian coordinate system is employed with the origin being located at the corner and mid-surface of the plate. Each k^{th} ply is rotated an arbitrary angle θ^k with respect to the x-axis as shown. The first-order shear deformation theory (FSDT) is applied together with the Lagrangian equations to derive the equations of motion for the plate. In this paper, only a brief account of these derivations is presented. For further details, the readers are referred to (Sone Oo *et al.* 2019, 2020).

According to FSDT, the following assumptions are made to derive the mechanical model of the plate:

- The transverse displacement is assumed to be independent of the thickness and the transverse normal strain is taken as zero.
- The transverse normal is allowed to rotate with respect to the mid-surface after the deformation.

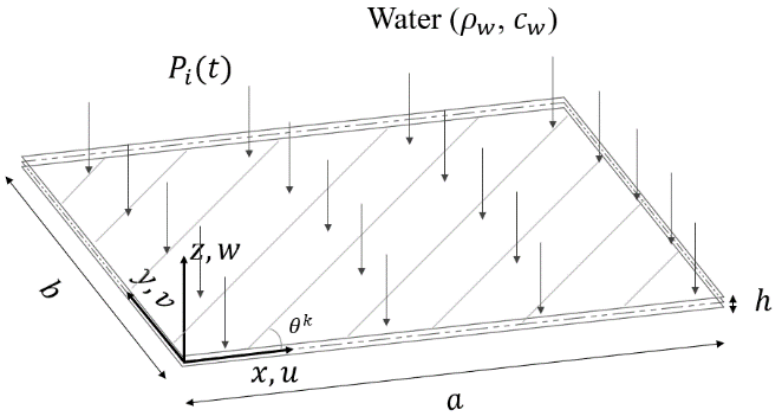

Fig. 2. Coordinate system and geometry of the rectangular plate

- Stress-strain relations obey generalized Hooke's law for orthotropic materials.
- Linear strain-displacement relations are considered.
- In-plane displacements are assumed negligibly small compared to the transverse displacement, i.e. $|u|, |v| \ll |w|$, thus reducing the problem from 5 degrees of freedom (5 DOFs) to 3 DOFs.
- In-plane and rotatory inertia are assumed negligibly small.
- Hydrostatic pressure, structural damping and the effects of failure are not considered.

To satisfy the simply-supported boundary conditions, Navier solution functions consisting of double Fourier summation can be adapted:

$$w(x,y,t) = \sum_{m=1}^{\infty}\sum_{n=1}^{\infty} W_{mn}\, sin\left(\frac{m\pi x}{a}\right) sin\left(\frac{m\pi y}{b}\right) \tag{17a}$$

$$\psi_x(x,y,t) = \sum_{m=1}^{\infty}\sum_{n=1}^{\infty} \Psi_{x_{mn}}\, cos\left(\frac{m\pi x}{a}\right) sin\left(\frac{m\pi y}{b}\right) \tag{17b}$$

$$\psi_y(x,y,t) = \sum_{m=1}^{\infty}\sum_{n=1}^{\infty} \Psi_{y_{mn}}\, sin\left(\frac{m\pi x}{a}\right) cos\left(\frac{m\pi y}{b}\right) \tag{17c}$$

where W_{mn}, $\Psi_{x_{mn}}$ and $\Psi_{y_{mn}}$ are three generalized coordinates, m and n are mode numbers in x- and y-directions respectively.

The time domain equation of motion for the plate is as follows:

$$\ddot{W}_{mn}(t) + \omega_{mn}^2 W_{mn}(t) = \frac{4}{A_f m_s} F_{mn}(t) \tag{18}$$

where $A_f = ab$ is the wet surface area of the plate, and the modal participation of the forcing term on the right-hand side of Eq. (18) can be expressed in terms of incident and scattered pressures as:

$$F_{mn}(t) = \int_0^b \int_0^a \left[\left(P_i(t) + P_s(x,y,t)\right) sin\left(\frac{m\pi x}{a}\right) sin\left(\frac{m\pi y}{b}\right)\right] dx\, dy \tag{19}$$

The natural frequency is $\omega_{mn} = \sqrt{K_{mn}/m_s}$, see Eq. (A1) of Appendix A to find the formulations of K_{mn}. Notice that the incident pressure is assumed to be evenly distributed across the plate and thus, does not depend on spatial coordinates. However, the scattered pressure is both a function of spatial and temporal variables. Assuming that the scattered pressure has the same mode shape functions as the transverse displacement,

$$P_s(x,y,t) = \sum_{m=1}^{\infty}\sum_{n=1}^{\infty} p_{mn}\, sin\left(\frac{m\pi x}{a}\right) sin\left(\frac{n\pi y}{b}\right) \tag{20}$$

In this case, a further assumption is imposed where DAA_1 from Eq. (5) is modified into:

$$\dot{P}_s(x,y,t) + D_f P_s(x,y,t) = \rho_w c_w(\dot{u}_i(t) - \ddot{w}(x,y,t)) \tag{21}$$

Substituting Eq. (20) into Eq. (21), multiplying both sides with the mode shape functions and then integrating both sides with respect to the surface area, the modal equation for the scattered pressure can be derived. On virtue of the orthogonality of the modes:

$$\int_0^b \int_0^a (\alpha_{mn}\alpha_{rs})\, dx\, dy = \begin{cases} \frac{A_f}{4}, & \text{if } m,n = r,s \\ 0, & \text{if } m,n \neq r,s \end{cases} \tag{22}$$

where $\alpha_{mn} = \sin(m\pi x/a)\sin(n\pi y/b)$, $\alpha_{rs} = \sin(r\pi x/a)\sin(s\pi y/b)$, and $m,n,r,s = 1,3,5,\ldots$ for the bi-symmetric problem (in both x- and y-axes).

The fluid modal equation derived using Eq. (21) is:

$$\dot{p}_{mn}(t) = -D_{f_{mn}} p_{mn}(t) - \rho_w c_w \ddot{W}_{mn}(t) + \left(\frac{16}{mn\pi^2}\right)\dot{P}_i(t) \tag{23}$$

Then, the force function from the right-hand side of eq. (18) becomes:

$$F_{mn}(t) = \left(\frac{4A_f}{mn\pi^2}\right)P_i(t) + \left(\frac{A_f}{4}\right)p_{mn}(t) \tag{24}$$

Using the same steps shown in the previous subsection, the following explicit equations are derived:

$$W_{mn}^{i+1} = W_{mn}^i \cos(\omega_{mn}\Delta t) + V_{mn}^i\left(\frac{\sin(\omega_{mn}\Delta t)}{\omega_{mn}}\right) - 4F_{mn}^i\left(\frac{\cos(\omega_{mn}\Delta t)-1}{A_f m_s \omega_{mn}^2}\right) \tag{25a}$$

$$V_{mn}^{i+1} = -W_{mn}^i \omega_{mn}\sin(\omega_{mn}\Delta t) + V_{mn}^i\cos(\omega_{mn}\Delta t) + 4F_{mn}^i\left(\frac{\sin(\omega_{mn}\Delta t)}{A_f m_s \omega_{mn}}\right) \tag{25b}$$

$$\dot{V}_{mn}^{i+1} = -\omega_{mn}^2 W_{mn}^i + \frac{4}{A_f m_s}F_{mn}^i \tag{25c}$$

$$p_{mn}^{i+1} = p_{mn}^i e^{-D_{f_{mn}}\Delta t} + \left(\frac{1-e^{-D_{f_{mn}}\Delta t}}{D_{f_{mn}}}\right)\left(-\rho c\dot{V}_{mn}^i + \rho c\dot{u}_i^i\left(\frac{16}{mn\pi^2}\right)\right) \tag{25d}$$

in which the initial conditions are taken the same as the previous rigid plate-spring system, i.e., $W(0) = V(0) = 0$, $\dot{V}(0) = 2P_0/m_s$ and $P_s(0) = P_i(0) = P_0$. Here, the constant term $D_{f_{mn}} = \rho_w c_w / M_{f_{mn}}$ should be calculated for each mode (m,n).

The water-added mass $M_{f_{mn}}$ is calculated using (Greenspon 1961)'s formulation as follows:

$$M_{f_{mn}} = \frac{1}{2}\rho_w b f(a/b) A_{mn}^2 \tag{26}$$

where $f(a/b) = 1.5(a/b)^3 - 3.12(a/b)^2 + 2.6(a/b) + 0.0098$ is the correction term for aspect ratios of the plate ($0 < f(a/b) \leq 1$) for $a \leq b$, and $A_{mn} = 8/(mn\pi^2)$ is the modal term (consisting of only odd numbered modes) for simply-supported boundary conditions. This added-mass formulation contains some approximations on the mode shape term and hence, is accurate only for the first mode shape and $A_{mn} = 0$ for even numbered modes.

The modal terms after solving Eqs. (25a) – (25d) are substituted into Eq. (17). Then, FSDT solution for the UNDEX response of a simply-supported rectangular orthotropic plate is obtained.

4. Preliminary results and analyses

The analytical equations from Section 3 are implemented in a MATLAB program. The obtained results are then confronted to those calculated by LS-DYNA/USA (DAA_1). Three different types of problems are studied: (1) spring-supported rigid plate subjected to a plane shock exponential wave, (2) simply-supported steel plate subjected to a uniformly distributed suddenly applied pressure load, and (3) simply-supported composite plate subjected to an exponentially decaying plane shock wave. The details about the finite element models are specified in each corresponding subsection.

4.1. Spring-supported rigid plate subjected to a plane shock exponential wave

A square rigid plate having the dimensions ($a = b = 167$ mm), uniform thickness ($h = 10$ mm), and density ($\rho_s = 1500$ kg.m^{-3}) is exposed to the water ($\rho_w = 1000$ kg.m^{-3}, c_w = 1498 m.s^{-1}) on one side. Four discrete springs possessing equivalent stiffness of $K = 4.5$ MN.m^{-1} are used to support the plate at corner nodes and on the other side of the plate. A single finite element rigid plate-spring model, resembling to the one depicted in Fig. 1, is constructed in LS-DYNA/USA (DAA_1). No fluid elements are modeled since the plate is coupled to DAA boundary element. Fully-integrated shell element formulation together with rigid material is applied.

A plane shock exponential wave comprised of a peak pressure $P_0 = 75$ MPa and decay time $\tau = 0.21$ ms is considered in the USA keyword input. Cavitation is treated approximately by limiting the total pressure at zero whenever it becomes negative. Here, both results with and without cavitation are shown just for the comparison purpose. However, it should be kept in mind that such treatment of cavitation on the fluid-structure interface is only an approximate approach, as shall be elaborated later. Results are calculated again using closed-form like analytical expressions given in Eqs. (15) and (16). Since the purpose is to test the validity of the developed equations, the same value of water-added mass, i.e., $M_f/m_s = 6.25$, obtained from LS-DYNA/USA (DAA_1) is used for the analytical calculation.

In Fig. 3, the results of displacement, velocity, acceleration, and normalized total pressure (P_{tot}/P_0) obtained from both LS-DYNA/USA (DAA_1) and analytical (DAA_1) are plotted as a function of time and up to 4 ms. As can be seen in all the plots, the analytical solutions are almost exactly the same as the numerical results using LS-DYNA/USA (DAA_1) with or without cavitation. In addition, the change in the behavior of the plate caused by the consideration of cavitation can be observed when the pressure has been cut-off at about 1.4 ms. Here, it is also worth mentioning that the authors tested the analytical formulations using other loading type (e.g., sinusoidal profile), and also with different acoustic impedance (e.g., air). In all the tests performed, almost the same results were found between analytical and numerical methods involving DAA_1. Therefore, it was concluded that the FSI coupling scheme works quite well for a single degree-of-freedom system.

4.2. Simply-supported steel plate subjected to a uniformly distributed suddenly applied pressure load

For the verification purpose, a simple case study is performed on a simply-supported isotropic (steel) plate subjected to a uniformly distributed suddenly applied pressure of 2.5 MPa. The characteristics of the steel plate are as shown in Table 1. A quarter plate model (50 mm $\times$ 50 mm) is constructed using a total of 169 fully-integrated shell elements along with elastic material model (MAT_001) from LS-DYNA. Five through thickness integration points are considered. A typical shear correction factor of 5/6 is applied. A symmetric boundary condition is applied to the inner edges of the plate while simply-supported (immovable) boundary is prescribed on the outer edges. Structural damping, material strain rate and the plastic effects are not included, making sure that the deflection remains small. The plate is coupled to DAA_1 boundary elements by specifying wet surface segments on the plate. A uniformly distributed suddenly applied incident pressure (P_0 = 2.5 MPa), also known as 'step loading', is applied via USA keyword input. Cavitation is also not considered in this analysis. The acoustic properties of water are taken as $\rho_w = 1025$ kg.m^{-3} and $c_w = 1500$ m.s^{-1}.

Table 1. Characteristics of the isotropic (steel) plate

$a = b$ (mm)	h (mm)	ρ_s (kg.m^{-3})	E (GPa)	ν	σ_y (MPa)
100	5.76	7800	200	0.3	240

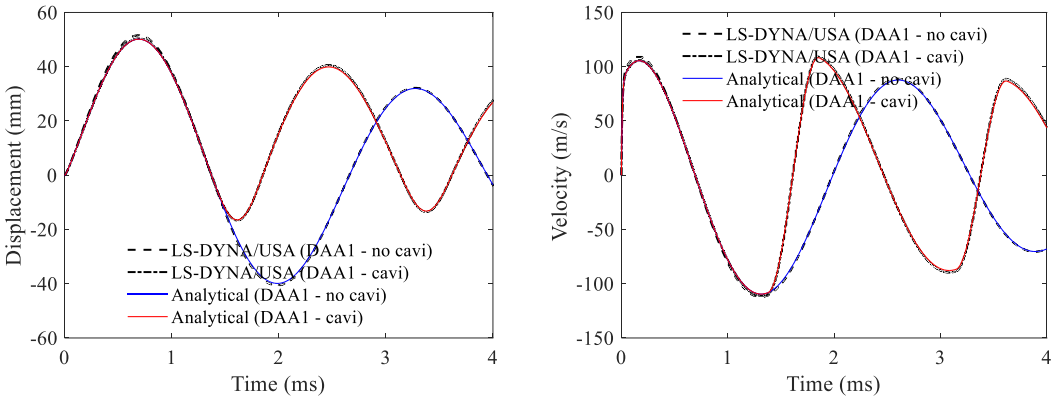

(a) Displacement-time history

(b) Velocity-time history

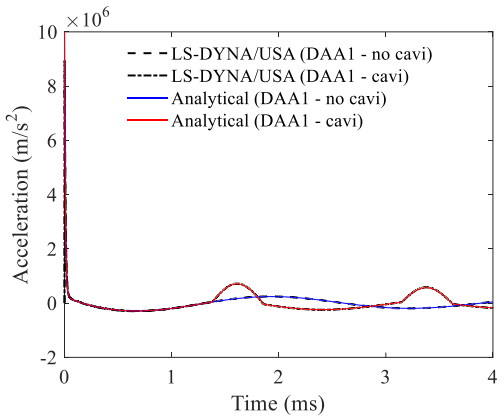

(c) Acceleration-time history

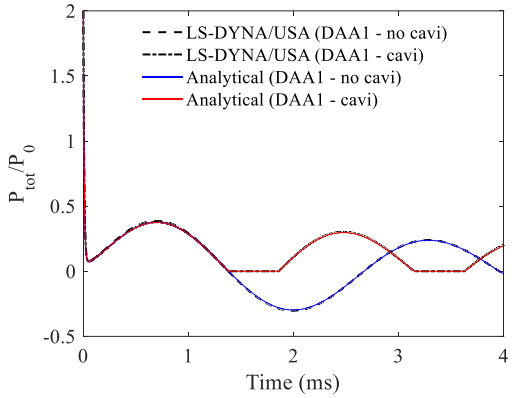

(d) Normalized total pressure-time history

Fig. 3. Comparison between LS-DYNA/USA and analytical results both using DAA$_1$ formulations (with/without cavitation)

The results of the central deflection and normalized total pressure are plotted as a function of time in Fig. 4. The analytical results include 6 modal participation terms, i.e., $m, n = 1, 3, 5, \ldots, 11$ (or $M = N = 6$). The general trends of both time history plots agree well with LS-DYNA/USA (DAA$_1$). The peak deflection at the center of the steel plate shows 4% discrepancy calculated with respect to the analytical peak value. A slight difference in the plate oscillation period can be observed. Moreover, small oscillations can be seen in the total pressure results calculated by the analytical approach. It was found out that such behavior in the analytical pressure results is mainly due to the insufficient water-added mass. As will be demonstrated in Section 5, the wetted natural frequencies of the analytical calculations are higher than those of LS-DYNA/USA (DAA$_1$). This means that the water-added mass given by Eq. (26) is insufficient. The small oscillations in the total pressure results are caused by the small water-added mass values (analytical) especially in the higher modes. According to Eq. (23), the scattered pressure depends on the constant D_{fmn}, recall that $D_{f_{mn}} = \rho_w c_w / M_{f_{mn}}$. Thus, the smaller $M_{f_{mn}}$ becomes, the larger is the value of D_{fmn}, leading to higher rate of change in the modal terms of the scattered pressure, i.e., $\dot{p}_{mn}$. The detailed studies as well as the improvement regarding the (areal) water-added mass calculations are given in Section 5. Note that the authors also checked the sensitivity of the results due to numerical damping (Rayleigh damping) in LS-DYNA/USA (DAA$_1$). It was found out that a recommended damping coefficient (by LS-DYNA user manual) between 0.1 – 0.25 yields nearly identical results, see Fig. B1 in Appendix B.

4.3. Simply-supported composite plate subjected to an exponentially decaying plane shock wave

A carbon-fiber/epoxy (CFRP) laminated plate having the same dimensions and thickness as the previous steel plate ($a = b = 100$ mm, $h = 5.76$ mm), and material density of 1548 kg.m^{-3} is considered here.

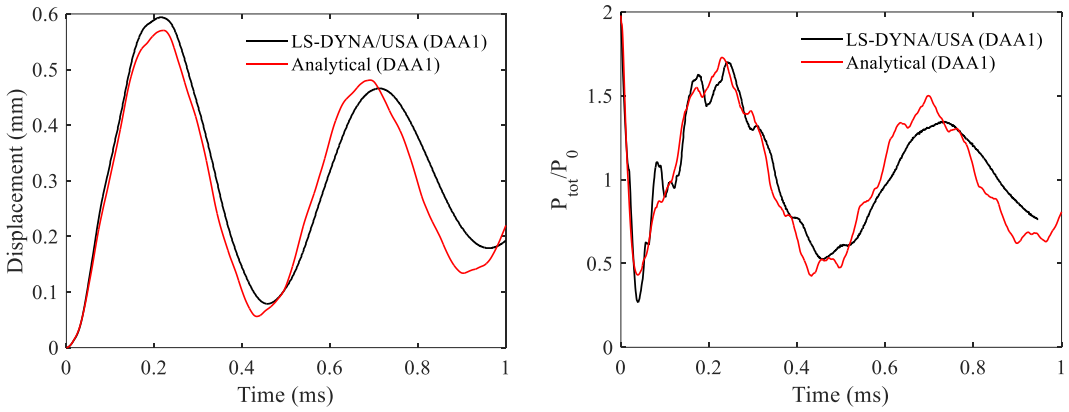

(a) Displacement-time history *(b) Normalized total pressure-time history*

Fig. 4. Preliminary comparison of steel plate response between LS-DYNA/USA (DAA$_1$) and analytical (DAA$_1$) approaches (Step loading: $P_0 = 2.5$ MPa; Both analytical and numerical approaches do not consider cavitation.)

The laminate consists of 20 plies with the stacking sequence of $[\pm 45/0/0/0/\pm 45/0/0/0/90/90]_S$, each ply making about 0.288 mm thickness. The material characteristics of the lamina used in CFRP plate are retrieved from the quasi-static tests performed by the authors, see Table 2. Only a quarter of the plate is modeled using symmetric boundary conditions. Simply-supported boundary conditions are applied to the plate's (outer) edges. The model employs 169 modified fully-integrated shell elements (EQ: -16) along with the composite material model (MAT_054), (LSTC 2017). Again, structural damping as well as damage effects are ignored in this analysis. An exponential incident shock wave having a peak pressure P_0 = 1.5 MPa and decay time τ = 1.3 ms is applied through DAA boundary elements. Note that this is the case where cavitation is supposed to be minimum since the load duration is relatively long compared to the plate response time. The acoustic properties of water are taken as ρ_w = 1025 kg.m^{-3} and c_w = 1500 m.s^{-1}. The authors have checked the mesh size sensitivity and the current result shown in this paper is the already converged one.

Table 2. Characteristics of the carbon-fiber/epoxy lamina

E_{11} (GPa)	$E_{22} = E_{33}$ (GPa)	$\nu_{12} = \nu_{13}$	ν_{23}	$G_{12} = G_{13}$ (GPa)	G_{23} (GPa)
138	8.98	0.281	0.385	3.66	3.24

Figure 5 shows the time evolutions of deflection, and normalized total pressure at the center of the plate. Numerical results obtained from LS-DYNA/USA (DAA$_1$) are with or without the cavitation. It can be seen that the effect of cavitation is not significant in this case since the two numerical results are nearly identical. Analytical results shown here consider up to12 modes $(M, N) = (12, 12)$. They are also more or less the same as results using $(M, N) = (6, 6)$. It should be noted that the number of modes participating could have some slight effect on the scattered pressure results as shall be seen later in Section 5. The authors also checked the sensitivity on the time step as well as shear correction factor on the analytical results. The results shown here used a time step of 1 μs, which is less than one-hundredth of the swing time ($T_0/100 \approx 3.2\ \mu s$) and the (total) shear correction factor used is 5/6.

In Fig. 4(a), the peak deflection is found around 0.32 ms and appears to be in good accordance with the numerical results. However, the period is slightly shorter for the analytical result than that of LS-DYNA/USA (DAA$_1$). As have already been observed in the case with steel plate, this is mainly due to the discrepancy in the water-added mass calculation between analytical and numerical results. LS-DYNA/USA (DAA$_1$) is found to have a larger water-added mass (with a relative error $\approx 12\%$) compared to the water-added mass given by (Greenspon 1961). These will be elaborated in the next section when natural frequencies up to the first four bending modes are compared in Table 3.

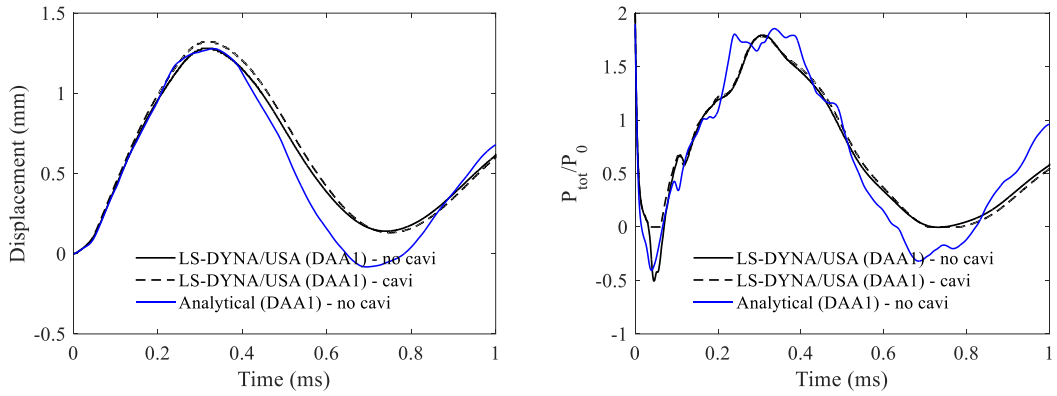

(a) Displacement-time history *(b) Normalized total pressure-time history*

Fig. 5. Comparison with LS-DYNA/USA and analytical results using DAA$_1$ formulations for CFRP plate

5. Investigations and improvement on the water-added mass formulation

5.1. Modification

The original water-added mass formulation proposed by (Greenspon 1961) assumed that the plate is made up of many small rectangular elements with equal area. The average pressure on a point caused by the vibration of any other points on the plate is approximated by supposing that the entire plate acts as a rectangular piston with a deflection equal to the average of the spatial term $\alpha_{mn}(x,y)$. It was claimed that such approximation is valid only for the first mode of the plate. According to Eq. (26), the water-added mass (per unit area) depends on the size and aspect ratio of the plate, the density of water and the square of the mode shape term A_{mn}^2. Therefore, to improve the formulation for higher modes, A_{mn}^2 from Eq. (26) need to be modified. Recall that,

$$A_{mn}^2 = \frac{64}{m^2 n^2 \pi^4} \tag{27}$$

which is independent of each mode. In this paper, by combining the modal index (m,n) from each direction x and y, Eq. (27) is modified as a summation form as $A_{mn}^2 = \sum_{j=1}^{\infty} 64/(mnj^2\pi^4)$, where $j = 1,3,5,\ldots$ is the odd numbered modal index. Note that the idea of adapting the summation form in calculating A_{mn}^2 is only an approximate attempt to slightly increase the value of the areal water-added mass at every mode. Hence, Eq. (26) becomes:

$$M'_{f_{mn}} = \frac{1}{2}\rho_w b f(a/b) \sum_{j=1}^{\infty} \frac{64}{mnj^2\pi^4} \tag{28}$$

Here, only the first 6 terms (i.e., $j = 1,3,\ldots,11$) are considered in the calculation of water-added mass. Since j^2 is in the denominator, using higher values of j in the series would not change the final result by a lot, as shall be shown.

In Fig. 6, the previous results on CFRP plate and the improved result using Eq. (28) are compared. LS-DYNA/USA (DAA$_1$) results are also plotted as reference. It can be seen that the small oscillations in the normalized total pressure-time plot disappear and the period of oscillation becomes more comparable to LS-DYNA/USA (DAA$_1$). As explained before, the increase in M_{fmn} would result in the decrease of D_{fmn} which in turn leads to smaller rate of change in the scattered pressure result according to Eq. (23). According to Fig. 6, the improvement causes only slight changes to the central deflection results.

5.2. Evaluations of the natural frequencies

Another improvement can be found in the (wet) natural frequencies. Table 3 shows comparison of natural frequencies up to the first four bending modes. In-air natural frequencies are also provided just

to compare. The inclusion of water-added effect decreases the in-air natural frequencies to half or even more than half in some cases. It can also be seen that even with the improvement, for some mode such as mode [3,3], there is still a large discrepancy up to about 22%.

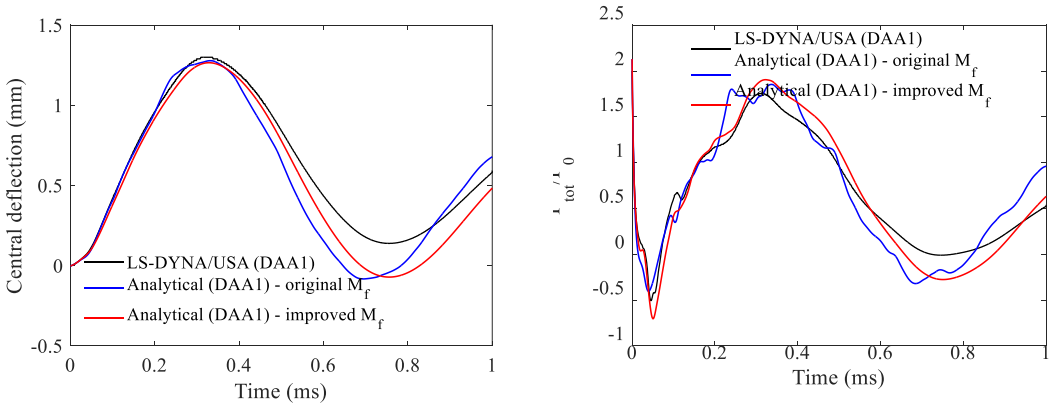

(a) Central deflection-time history *(b) Normalized total pressure-time history*

Fig. 6. Comparison between original and improved formulations of water-added mass (using CFRP plate, $P_0 = 1.5$ MPa, $\tau = 1.3$ ms)

Table 3. Comparison of natural frequencies (up to the first four bending modes)

			Natural frequencies in-air			Natural frequencies in-water			Discrepancy	
Material	a/h	Mode	Analytical	Numerical	Discrep.[1]	Numerical	Ana. original[2]	Ana. improved[3]	Original	Improved
			Hz	Hz	%	Hz	Hz	Hz	%	%
Steel	69	[1,1]	173	173	0.1%	80	87	81	8%	1.7%
		[1,3]	864	870	-0.7%	585	748	584	22%	-0.3%
		[3,1]	864	870	-0.7%	585	748	584	22%	-0.2%
		[3,3]	1552	1553	-0.1%	1174	1524	1313	23%	11%
	17	[1,1]	2747	2736	1.1%	1953	2077	1997	6%	2.2%
		[1,3]	13258	13420	-0.9%	11653	12738	11638	9%	-0.1%
		[3,1]	13258	13427	-1.0%	11653	12738	11638	9%	-0.1%
		[3,3]	23087	22971	-0.1%	21185	22981	22020	8%	3.8%
CFRP	69	[1,1]	191	190	0.5%	43	48	44	10%	2.7%
		[1,3]	673	669	0.6%	259	411	254	37%	-1.9%
		[3,1]	1220	1216	0.3%	472	745	461	37%	-2.4%
		[3,3]	1672	1652	1.2%	754	1535	965	51%	22%
	17	[1,1]	2906	2807	3.4%	1172	1330	1239	12%	5.4%
		[1,3]	9620	9431	2.0%	6037	8074	6083	25%	0.8%
		[3,1]	14661	14456	1.4%	9258	12305	9271	25%	0.1%
		[3,3]	19518	18965	2.8%	13546	19078	15935	29%	15%

[1] *where all the discrepancies are calculated using the formula,* $Discrep. = \frac{Analytical - Numerical}{Analytical} \times 100\%$.

[2] *Ana. original - Analytical calculation using original water-added mass formulation proposed by* (Greenspon 1961), *Eq. (26).*

[3] *Ana. improved - Analytical calculation using improved water-added mass formulation, Eq. (28).*

5.3. Sensitivity to the number of mode shapes

The use of summation form in the water-added mass calculation does not make a closed-form expression, and thus, the effect of the number of modal terms is investigated. The case with a steel plate model defined in Subsection 4.2 is utilized in this case. As plotted in Fig. 7, using different number of modal terms does not change the results a lot. In fact, the central deflections are almost identical. The normalized scattered pressures are only slightly affected at the beginning of the calculation. According to the initial condition, the scattered pressure at time $t = 0$ should be $P_s(0) = P_0$. However, The Fourier series decomposition of P_s shown in Eq. (20) could satisfy such a condition only after taking into account many modes, for instance, $M = N = 30$. Even so, the overall behavior in the longer time converges regardless of the number of modes ($M, N \geq 3$) according to the results shown.

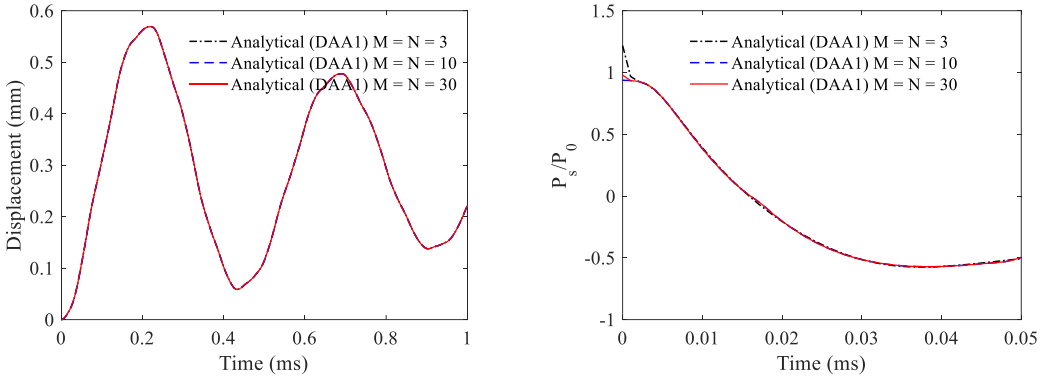

(a) Central deflection-time history *(b) Normalized scattered pressure-time history*

Fig. 7. Effect of the number of modal terms in analytical (DAA$_1$) approach (using steel plate, step loading of 2.5 MPa)

6. Parametric studies

In this section, the effect of changing the aspect ratios and the loading levels is studied using the material models presented before. The problem domain is divided into two: (1) steel plate responses under varying levels of step loadings, and (2) composite plate responses under different exponential loadings. Two different sizes of the plate are adapted and termed as 'thin' plate and 'thick' plate. Thin plate has the dimension of $a = b = 400$ mm while thick plate possesses $a = b = 100$ mm. Same thickness of 5.76 mm is used in all cases. As before, cavitation or damage is not included in the study. Note also that an improved water-added mass formulation, Eq. (28), and up to 6 modal terms $(M = N = 6)$ are considered in all the coming analyses.

6.1. Steel plate responses under varying levels of step loadings

In Fig. 8, maximum central deflection-thickness ratios (w_{max}/h) for thin and thick steel plates are plotted as a function of the step pressures P_0. As expected, the analytical (DAA$_1$) results are linearly proportional to the peak pressures and valid until the geometric nonlinearity involves. It can be seen in Fig. 8(a) that the geometric nonlinearity effect is more significant for thin plate (large a/h ratio) due to lower stiffness. The thick plate (small a/h ratio) appears to withstand linearly much higher pressures accompanied by lower w_{max}/h results. A relative error of $\pm 15\%$ is shown in both plots and it can be said that the current analytical (DAA$_1$) results correlate well with those of LS-DYNA/USA (DAA$_1$) only up to $w_{max}/h \leq 0.5$. Exceeding this value would need to incorporate geometric nonlinear effect (by moderate rotation) into the formulations. The issue has actually been investigated and resolved but, for conciseness, the corresponding nonlinear developments and results will be published in the next paper.

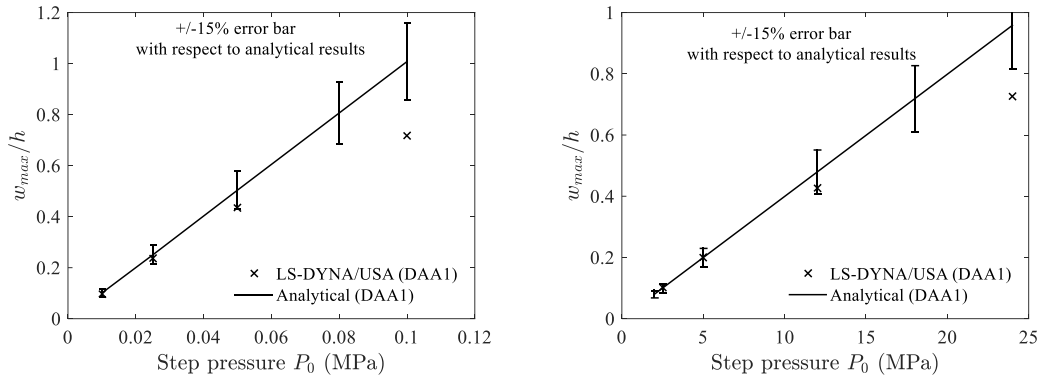

(a) Thin steel plate ($a/h = 69.4$) *(b) Thick steel plate ($a/h = 17.4$)*

Fig. 8. Comparison of the responses of (a) thin steel plate (a/h = 69.4), and (b) thick steel plate (a/h = 17.4) loaded by varying levels of suddenly applied step pressures using LS-DYNA/USA (DAA_1) and analytical (DAA_1) approaches

6.2. Composite plate responses under different exponential loadings

Thin and thick CFRP plates, whose material characteristics are given in Table 2, are subjected to different levels of exponential loading comprised of various combinations of peak pressures and decay times as shown in Table 4. It should be noted that some of these load cases are only hypothetical. The charge masses and the standoff distances are selected in order to give the same transferred impulse I_t calculated by Taylor's simplified FSI formulation (Taylor 1941). The load cases from C-1a to C-1d represent thin CFRP plate while those from C-2a to C-2f analyzes for thick CFRP plate. Four different results using: (1) LS-DYNA/USA (DAA_1) with cavitation and (2) LS-DYNA/USA (DAA_1) without cavitation, (3) analytical (DAA_1) without cavitation, and (4) analytical (two-step) approach are compared. Detailed formulations and assumptions of analytical (two-step) approach can be found in (Sone Oo *et al.* 2020).

Table 4. Load cases performed for carbon-fiber/epoxy thin and thick plates

	Plate characteristics		Characteristics of explosives (TNT)			Loadings		FSI parameter and impulse		
Cases	a/h (-)	f_0 (Hz)	C (kg)	R (m)	$S.F$	P_0 (MPa)	τ (ms)	I_0 (Ns.m^{-2})	ψ	I_t (Ns. m^{-2})
C-1a	69.4	190	0.02	11.66	0.013	0.647	0.050	32.4	8.6	5.66
C-1b	69.4	190	0.77	43.37	0.020	0.551	0.167	91.8	28.7	5.66
C-1c	69.4	190	6.12	90.19	0.027	0.524	0.335	175.4	57.7	5.66
C-1d	69.4	190	48.29	184.03	0.038	0.509	0.670	340.9	115.5	5.66
C-2a	17.4	2808	0.00	2.36	0.029	2.3	0.024	55.9	4.2	17.02
C-2b	17.4	2808	0.04	5.52	0.036	1.939	0.051	98.2	8.7	16.99
C-2c	17.4	2808	1.97	23.61	0.059	1.632	0.192	313.5	33.1	16.97
C-2d	17.4	2808	24.68	57.26	0.087	1.55	0.450	696.9	77.5	16.98
C-2e	17.4	2808	196.11	116.57	0.120	1.514	0.901	1363.4	155.3	17.00
C-2f	17.4	2808	586.94	169.32	0.143	1.5	1.300	1949.5	224.1	16.98

where a/h is the aspect ratio of the plate, $f_0 = \omega_{11}/(2\pi)$ is the fundamental natural frequency (mode 1,1) of the plate, $S.F = \sqrt{C}/R$ is the shock factor, P_0 is the peak pressure, τ is the decay time, $I_0 = P_0\tau$ is the applied impulse related to the incident wave, $\psi = \rho_w c_w \tau/m_s$ is the FSI coefficient associated to the decay time and areal mass of the plate, $I_t = 2I_0\psi^{-\psi/(\psi-1)}$ is the reduced transferred impulse due to the FSI effect given by (Taylor 1941).

The two-step approach can be summarized as follows (Sone Oo *et al.* 2020):

- In the first step (early-time phase), the impulsive velocity is calculated by $v_i = I_t/m_s$, where $I_t = 2I_0\psi^{-\psi/(\psi-1)}$, $\psi = \rho_w c_w \tau/m_s$ and $m_s = \rho_s h$.
- In the second step (long-time phase), the free response of the plate is determined by using the first-order shear deformation theory while taking into account the water-added inertia effect.

According to the study shown in (Sone Oo et al. 2020), the applicable domain of the analytical (two-step) approach is:

- For $a/h = 69.4 : 0.09 \leq \tau/T_0 \leq 0.16$ $(19.8 \leq \psi \leq 34.5)$, and
- For $a/h = 17.4 : 0.28 \leq \tau/T_0 \leq 0.35$ $(4.0 \leq \psi \leq 5.1)$.

where $T_0 \approx 1/f_0$ is the natural period of the plate. It is worth mentioning here that these ranges of validity were deduced based on the results of LS-DYNA/USA (acoustic) simulation results. Unlike the surface approximation model such as DAA, LS-DYNA/USA (acoustic) approach incorporates the fluid elements so that cavitation appearing near the plate can be properly accounted for. An interesting fact about using such method which utilizes acoustic fluid is that it has been validated by experiments, see (Sone Oo *et al.* 2020) for details. However, they are much more expensive and time consuming compared to LS-DYNA/USA (DAA_1) or analytical approaches due to the need for fine fluid mesh. Therefore, in what follows, only the results of analytical (two-step) approach will be shown, keeping in mind about the range of validity mentioned above.

6.2.1. Sensitivity to varying the FSI parameter ψ

Analyses are performed on different load cases shown in Table 4. Comparison is done on the same areal mass of the plate. The results are plotted in Figs. 9 and 10 for thin and thick CFRP plates respectively. The following dimensionless parameter for peak central deflection is introduced so as to make a more generalized interpretation of the results:

$$\overline{W}_{max} = \frac{w_{max}}{w_{taylor}} = \frac{\rho_w c_w}{2P_0\tau} w_{max} \tag{29}$$

where $w_{taylor} = 2P_0\tau/(\rho_w c_w)$ is the maximum displacement if cavitation is not accounted at all, that is, by assuming that water can support tension (Taylor 1941).

In Fig. 9, when cavitation flag is on, LS-DYNA/USA (DAA_1) overestimates in all cases regardless of the parameter ψ. In fact, such behavior is doubtful for two reasons: (1) in terms of the shock energy carried by the incident shock wave, the internal energy results evaluated from LS-DYNA/USA (DAA_1) are almost one order magnitude larger than the value obtained from similitude equation given by (Cole 1948) [4], and (2) the valid region (shown by red-colored dotted box in Fig. 9) for the analytical (two-step) approach are only about half of the results of LS-DYNA/USA (DAA_1) with cavitation. In addition, there have also been some evidence in which LS-DYNA/USA (DAA_1) with cavitation option overestimates the response by about 30 - 40% in comparison with the experiments (Sone Oo *et al.* 2020). One possible explanation of such overestimation is that LS-DYNA/USA (DAA_1) considers an approximate treatment of cavitation only on the fluid-structure interface, that is, when the total pressure at a spatial point falls below zero, the scattered pressure is modified as have already demonstrated in Subsection 4.1. Once the cavitated zone collapses, the water-added inertia effect might have possibly kicked in, leading to such overestimations. Indeed, this kind of approximate treatment used by LS-DYNA/USA (DAA_1) does not take into account the propagation and arrest of the breaking and closing fronts which are the phenomena of cavitation observed in fluid (Kennard 1943). Some of the fluid energy (or water-added inertial effect) may have already lost during such activity. This issue needs to be further investigated in the future.

Apart from the cavitation model, it is expected that analytical (DAA_1) model should correlate well with LS-DYNA/USA (DAA_1) model if cavitation is disregarded. However, the current formulation when applied for the thin plate seems to correlate well only around $\psi = 28.7$ $(\tau/T_0 = 0.13)$. By reducing the

[4] To put a sense of the magnitudes involved, consider the case of C-1a in which the shock wave energy given by empirical relation, $E_0 = K_4 C^{1/3}\left(C^{1/3}/R\right)^{A_4}$, is only about 3.7 J ($= E_0 * A_f$) while the internal energy of the plate in numerical model (with cavitation) is about 27.73 J. In terms of the energy ratio, numerical model (DAA_1) with cavitation model shows about 7.5 times more than the energy carried by the incident shock wave. In another test performed on the same case study by using LS-DYNA/USA with acoustic fluid elements, the internal energy is only about 0.8 J ($< E_0 = 3.7$ J) which makes more sense.

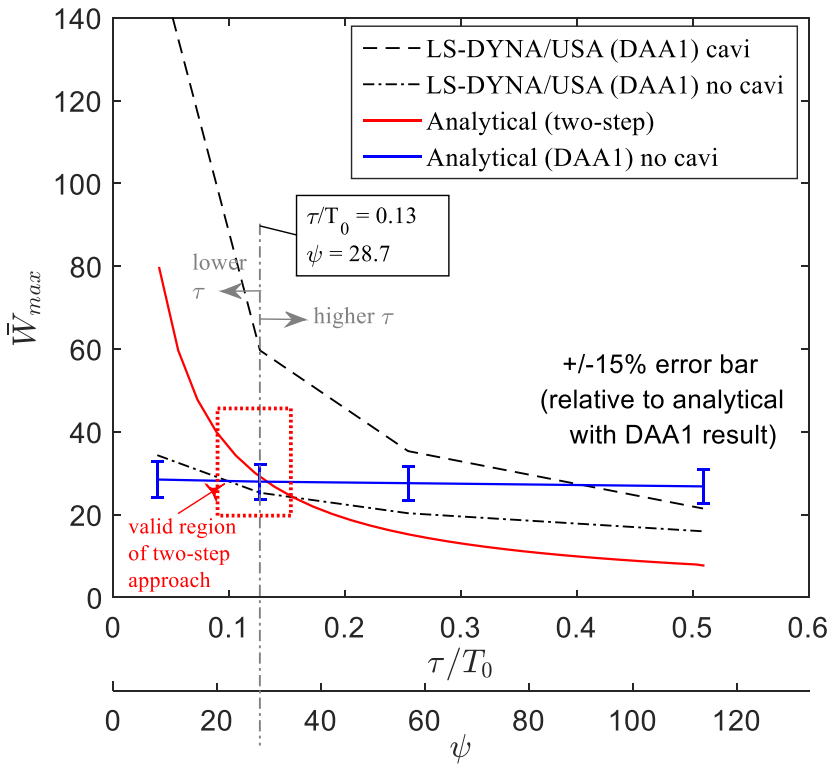

Fig. 9 Sensitivity to change of FSI parameter ψ on the response of thin CFRP plate (a/h = 69.4, cases C-1a to C-1d)

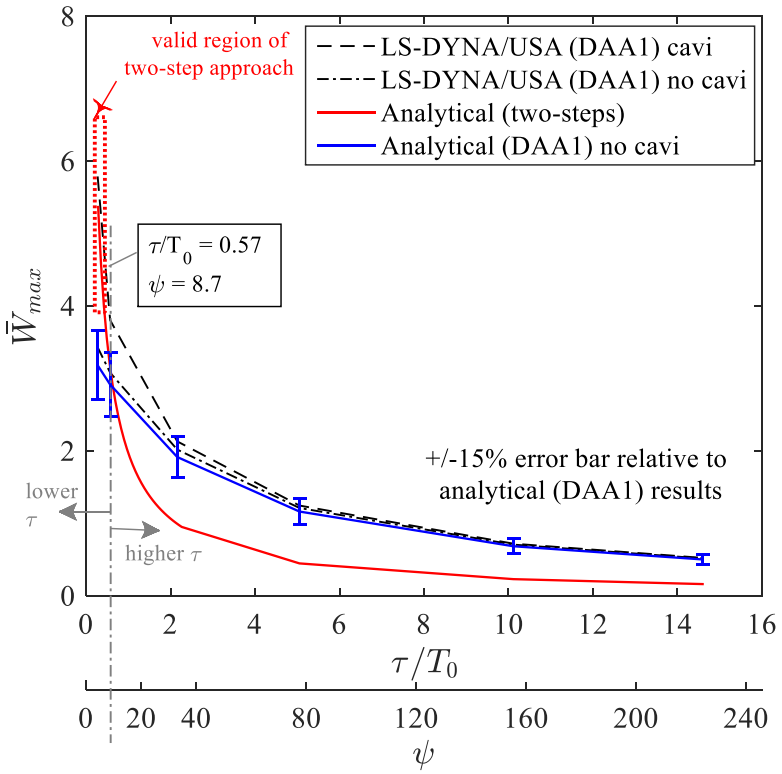

Fig. 10. Sensitivity to change of FSI parameter ψ on the response of thick CFRP plate (a/h = 17.4, cases C-2a to C-2f)

value of τ, the FSI parameter ψ decreases. If $\psi < 28.7$, cavitation becomes important and the current model is no longer valid because of the large negative pressures which create non-physical suction effect to the plate, resulting in the decrease of the amplitude. When $\psi > 28.7$ which is outside the valid region of two-step analytical approach, the analytical (DAA_1) formulae should predict the peak deflection well if and only if the central deflection does not exceed 0.5 times the thickness. The load cases (C-1c and C-1d) are unable to satisfy this requirement because of the involvement of higher shock factors as well as the flexibility of the relatively thin plate. This observation can be readily checked by fixing the decay time and changing only the peak pressures. This is confirmed and shown in Fig. 11(a) which will be explained in the subsequent subsection.

In contrast to Fig. 9, the results of analytical (DAA_1) results plotted in Fig. 10 correspond better to the LS-DYNA/USA (DAA_1) results without cavitation option. This is because the maximum deflection is relatively small for thick plate (case studies: C-2a to C-2f) and remains well within the small deflection domain. Another observation is that LS-DYNA/USA (DAA_1) with cavitation begins to converge to those without cavitation after about $\tau/T_0 \approx 2.1$ ($\psi \approx 33$). This means that cavitation is not as important as in the case of the more flexible plate (with large a/h). Indeed, this kind of observation has been identified in the previous paper of (Sone Oo *et al.* 2020) as well. Moreover, it can be seen that the analytical (two-steps) approach quickly leads to underestimations of the response because the transferred impulse given by Taylor's formulation is no longer sufficient to capture the continuing action of the FSI. In this regard, applying analytical (DAA_1) approach allows one to capture the response more correctly as compared to the impulse-based (two-step) analytical approach proposed in (Sone Oo *et al.* 2020).

6.2.2. Sensitivity to varying the peak pressure P_0

In Fig. 11, the comparisons are again carried out by varying the peak pressures but keeping the same decay time. As have already been observed before, both analytical results are linearly proportional to the peak pressures. LS-DYNA/USA (DAA_1) with cavitation results are not plotted anymore here since the selected decay times are relatively high and within the region where the effect of cavitation may be disregarded (i.e., the FSI parameter ψ is relatively large for both cases). As can be seen, these are also the regions where the previously proposed analytical formulations using two-step calculation approach are not valid anymore and they will always underestimate the response compared to coupled DAA_1 approaches. In Fig. 11(a), the analytical (DAA_1) results are comparable (within $\pm 15\%$ relative error) to numerical results only when $w_{max}/h < 0.5$, i.e., small applied impulse ($I_0 < 50$ Ns.m^{-2}), leading to small linear deflection. On the other hand, the results with the thick plate shown in Fig. 11(b) are in much better accordance with LS-DYNA/USA (DAA_1) results since the peak deflection is well within small deflection range.

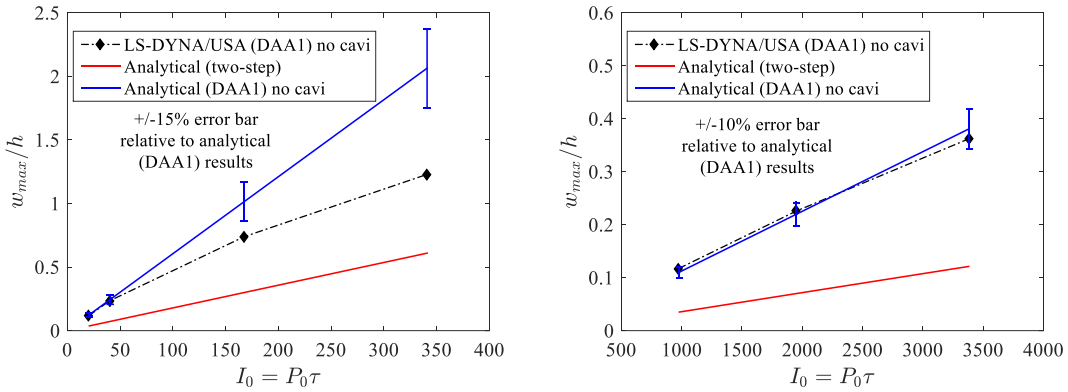

(a) Thin CFRP plate ($a/h = 69.4$) at $\psi = 115.5$ *(b) Thick CFRP plate ($a/h = 17.4$) at $\psi = 224.1$*

Fig. 11. Sensitivity to varying the peak pressure P_0 on (a) thin CFRP plate ($a/h = 69.4$), and (b) thick CFRP plate ($a/h = 17.4$)

7. Conclusions and perspectives

In this paper, the first order Doubly Asymptotic Approximation is coupled to the analytical structural equations to predict the underwater blast response of spring-supported rigid plate and simply-supported deformable plates. Air-backed condition is considered for both cases. Structural damping, hydrostatic pressure as well as material damage effects are disregarded. Uniformly distributed dynamic step loading and plane shock exponential loadings are applied. Nonstandard finite difference (NSFD) scheme is used to derive the closed form like analytical solutions. The obtained analytical results are preliminarily tested on rigid plate as well as isotropic and composite plates and are confronted against LS-DYNA/USA (DAA_1) results without cavitation. As for the rigid plate-spring system, the results agree excellently with those from LS-DYNA/USA (DAA_1) simulation. The deformable model, however, shows some oscillations especially in the total pressure results. After comparisons of the first four natural frequencies, the water-added mass formulation proposed by (Greenspon 1961) is slightly modified to improve its accuracy especially for the higher oscillation modes. Such improvement, however, is not rigorously justified and thus, needs more investigation in the future.

Parametric studies are also performed by varying the aspect ratios of the plate as well as the loading levels. To make effective evaluations, previous analytical results based on two-step approach are also given in addition to the LS-DYNA/USA (DAA_1) results with and without cavitation. According to the various case studies performed in this paper,

- the current analytical result with DAA_1 is linearly proportional to the applied peak pressures and valid only before the geometric nonlinearity becomes significant, that is, the peak central deflection is less than half the plate thickness,
- changing the decay time would change the FSI parameter ψ as well as the time ratio between the decay time of the loading and the plate fundamental period of oscillation (τ/T_0), which in turn could lead to a change in the action of cavitation,
- flexible thin plates with large aspect ratio are prone to be more influenced by cavitation as well as geometric nonlinear effect (large deflection) as compared to thick plates with small aspect ratio, and
- the current method is only able to capture the peak deflection when cavitation is not important and the deflection remains well within linear elastic domain.

According to these observations and conclusions, it is obvious that the current analytical model needs three immediate improvements regarding: (1) the action of cavitation, (2) the involvement of geometric nonlinear effects caused by moderate or large rotation (In fact, this issue has already been investigated and resolved but, for conciseness, the corresponding nonlinear developments and results will be published in another paper), and (3) the possible influence of the first ply damage and post-damage behavior. In addition, it would be of academic interest to see if the current approach can be extended for the different boundary conditions and geometries such as stiffened plates and curved panels. These topics will be left for the future studies.

Nevertheless, it is worth pointing out that the advantages of the proposed analytical formulations lie in the computational time and their reasonable accuracy (i.e., $< \pm 15\%$ relative error) if applied in the valid range. To highlight its potential, a brief comparison is made between the typical computation time using analytical (DAA_1), LS-DYNA/USA (DAA_1) and LS-DYNA/USA (acoustic) approaches and shown in Table 5. Note that these are solved on the same computer (Core i7-8550U @1.8GHz, RAM 16 GB). The associated termination time and the degrees of freedom (DOFs) are listed as well. As can be seen, the analytical approach takes little or no time to finish the calculations while the numerical approaches can be much more expensive depending on the number of DOFs involved. Therefore, the analytical approach may well be used especially in the pre-design stages where different lamination schemes, different loadings as well as plate geometry optimizations need to be performed.

Table 5. Comparison of the typical computation time between analytical (DAA_1), LS-DYNA/USA (DAA_1) and LS-DYNA/USA (acoustic) approaches

Case	Termination	Analytical (DAA_1)		LS-DYNA/USA (DAA_1)		LS-DYNA/USA (acoustic)	
	time (ms)	DOF	Time (s)	DOF	Time (s)	DOF	Time (s), (HH:MM:SS)
Thin CFRP plate	8	3	2.40	4681	208	5,131,227	12362 (03:26:02)
Thick CFRP plate	5	3	1.96	1345	96	304,572	356 (00:05:56)

The data for thin CFRP plate was taken from case study C-1d, and for thick CFRP plate, they were from case C-2f.

Acknowledgements

This research work has been granted financially by DGA Naval Systems, France within the framework of the project SUCCESS. The authors would also like to express their gratitude to Calcul-Meca and Multiplast companies for their technical assistance, and also to the reviewers and organizers of the ICSOS conference. Last but not least, the authors would like to thank Marc E. Songolo from ICAM for his helpful advice during the development of the mathematical model.

Appendix A. Calculation of stiffness K_{mn}

The stiffness K_{mn} is calculated as:

$$K_{mn} = K_{11} + \frac{2K_{12}K_{23}K_{13} - K_{12}^2K_{33} - K_{13}^2K_{22}}{K_{22}K_{33} - K_{23}^2} \tag{A1}$$

The stiffness terms K_{ij} (where $i, j = 1, 2, 3$) are expressed as follows:

$$K_{11} = A_{44}\left(\frac{n\pi}{b}\right)^2 + A_{55}\left(\frac{m\pi}{a}\right)^2 \tag{A2}$$

$$K_{12} = A_{55}\left(\frac{m\pi}{a}\right) \tag{A3}$$

$$K_{13} = A_{44}\left(\frac{n\pi}{b}\right) \tag{A4}$$

$$K_{22} = D_{11}\left(\frac{m\pi}{a}\right)^2 + D_{66}\left(\frac{n\pi}{b}\right)^2 + A_{55} \tag{A5}$$

$$K_{23} = \frac{mn\pi^2}{ab}(D_{11} + D_{66}) \tag{A6}$$

$$K_{33} = D_{22}\left(\frac{n\pi}{b}\right)^2 + D_{66}\left(\frac{m\pi}{a}\right)^2 + A_{44} \tag{A7}$$

where D_{11}, D_{22}, D_{66} are bending stiffnesses and A_{44}, A_{55} are shear stiffnesses. Their corresponding formulations can be found in any classical composite textbooks, for example (Reddy 2004).

Appendix B. Sensitivity to numerical damping in LS-DYNA/USA (DAA_1)

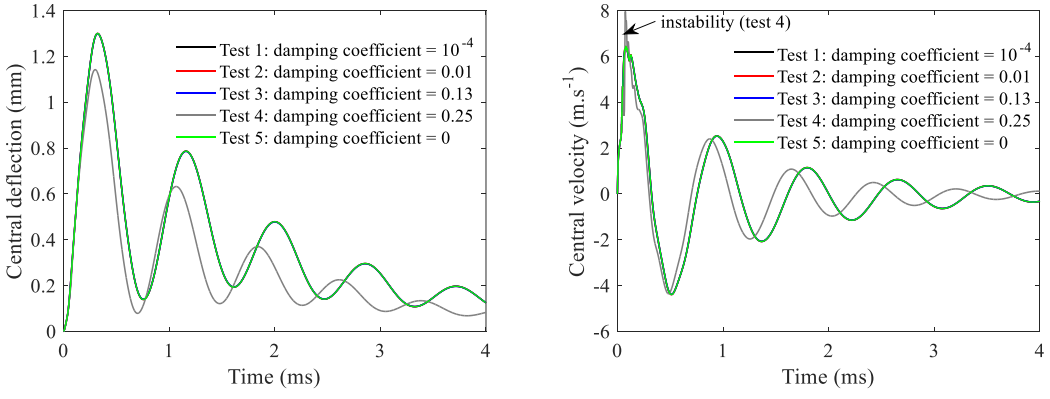

(a) Central deflection-time history *(b) Central velocity-time history*

Fig. B1. Sensitivity regarding numerical damping (Rayleigh stiffness damping coefficients) on LS-DYNA/USA (DAA_1) results

References

Barras, G. 2012. "Interaction Fluide-Structure: Application aux Explosions Sous-Marines en Champ Proche." University of Sciences and Technologies, Lille, France.

Blevin, R.D. 1979. *Formulas for Natural Frequency and Mode Shape*. New York: Van Nostrand Reinhold Co.

Brochard, K., Le Sourne, H., and Barras, G. 2018. "Extension of the String-on-Foundation Method to Study the Shock Wave Response of an Immersed Cylinder." *International Journal of Impact Engineering* 117 (May 2017): 138–52. https://doi.org/10.1016/j.ijimpeng.2018.03.007.

Brochard, K., Le Sourne, H., and Barras, G. 2020. "Estimation of the Response of a Deeply Immersed Cylinder to the Shock Wave Generated by an Underwater Explosion." *Marine Structures* 72 (January).

Cole, R.H. 1948. *Underwater Explosions*. Princeton: Princeton University Press.

DeRuntz, J.A. Jr. 1989. "The Underwater Shock Analysis Code and Its Applications." In *Proceedings of the 60th Shock and Vibration Symposium*: 89–107.

Deshpande, V.S., Heaver, A., and Fleck, N.A. 2006. "An Underwater Shock Simulator." In *Proceedings of the Royal Society A*, Cambridge, UK, 1021–41.

Geers, T.L. 1978. "Doubly Asymptotic Approximations for Transient Motions of Submerged Structures." *The Journal of the Acoustical Society of America* 64: 1500–1508.

Greenspon, J.E. 1961. "Vibrations of Cross-Stiffened and Sandwich Plates with Application to Underwater Sound Radiators." *The Journal of the Acoustical Society of America* 33(11): 1485–97.

Hutchinson, J.W., and Xue, Z. 2005. "Metal Sandwich Plates Optimized for Pressure Impulses." *International Journal of Mechanical Sciences* 47(4-5 SPEC. ISS.): 545–69.

Kennard, E.H. 1943. "Cavitation in an Elastic Liquid." *Physical Review* 63(5 and 6): 172–81.

LSTC. 2017. *LS-DYNA Keyword User's Manual, Volume I*. California, US.: Livermore Software Technology Corporation (LSTC). www.lstc.com.

Mickens, R.E. 1993. *Nonstandard Finite Difference Models of Differential Equations*. World scientific. https://www.worldscientific.com/doi/abs/10.1142/2081.

Reddy, J.N. 2004. *Mechanics of Laminated Composite Plates and Shells*. 2nd ed. Florida: CRC Press LLC.

Schiffer, A., and Tagarielli, V. L. 2015. "The Response of Circular Composite Plates to Underwater Blast: Experiments and Modelling." *Journal of Fluids and Structures* 52: 130–44. http://dx.doi.org/10.1016/j.jfluidstructs.2014.10.009.

Schiffer, A., Tagarielli, V.L., Petrinic, N., and Cocks, A. 2012. "The Response of Rigid Plates to Deep Water Blast : Analytical Models and Finite Element Predictions." *Journal of Applied Mechanics* 79.

Sone Oo, Y. P., Le Sourne, H., and Dorival, O. 2020. "On the Applicability of Taylor ' s Theory to the Underwater Blast Response of Composite Plates." *International Journal of Impact Engineering* 145(July): 1–15. https://doi.org/10.1016/j.ijimpeng.2020.103677.

Sone Oo, Y. P., Le Sourne, H., and Dorival, O. 2019. "Development of Analytical Formulae to Determine the Response of Submerged Composite Plates Subjected to Underwater Explosion." In *The 14th International Symposium on Practical Design of Ships and Other Floating Structures - PRADS 2019*, Yokohama, Japan, 1–21.

Songolo, M.E., and Bidégaray-Fesquet B. 2018. "Nonstandard Finite-Difference Schemes for the Two-Level Bloch Model." *International Journal of Modeling, Simulation, and Scientific Computing*

9(4): 1–23.
Taylor, G.I. 1941. “The Pressure and Impulse of Submarine Explosion Waves on Plates.” In *The Scientific Papers of G. I. Taylor, Vol. III*, Cambridge, UK: Cambridge University Press, 287–303.